ELSEVIER

Journal of Applied Geophysics 46 (2001) 235–248

JOURNAL OF APPLIED GEOPHYSICS

www.elsevier.nl/locate/jappgeo

# Analysis and interpretation of anomalous conductivity and magnetic permeability effects in time domain electromagnetic data Part II: $S\mu$-inversion

Michael S. Zhdanov *, Dmitriy A. Pavlov

*Department of Geology and Geophysics, College of Mines and Earth Sciences, University of Utah, 135 S 1460 E, Room 719, Salt Lake City, UT 84112-0111, USA*

Received 11 January 2000; accepted 8 March 2001

**Abstract**

In the paper by Pavlov and Zhdanov [J. Appl. Geophys. (2001)], we demonstrated that anomalous magnetic permeability of an ore body could result in measurable anomalous effects in TDEM data, which can be used in geophysical exploration. In the current paper, we develop a new method of TDEM data interpretation, which allows simultaneous reconstruction of both electrical and magnetic properties of the rocks. The method is based on a generalization of the $S$-inversion technique [66th Ann. Int. Mtg., Soc. Expl. Geophys., Expanded Abstr. (1996) 1306; 68th Ann. Int. Mtg., Soc. Expl. Geophys., Expanded Abstr. (1998) 473; J. Appl. Geophys. (1999)] for models containing thin sheets with anomalous conductivity and anomalous magnetic permeability. We call this method $S\mu$-inversion. Numerical 3-D modeling results demonstrate that $S\mu$-inversion provides useful information about both subsurface conductivity and magnetic permeability distributions. It can be used as a new tool for imaging TDEM data in mineral exploration. 

*Keywords:* Conductivity; Permeability; Time-domain electromagnetic method; Inversion

## 1. Introduction

In a preceding paper (Pavlov and Zhdanov, 2001), we studied transient electromagnetic field propagation through a medium containing bodies with both anomalous conductivity and anomalous magnetic permeability. The remarkable result was that the combination of anomalous conductivity and permeability within the same body increased significantly the anomalous TDEM response in comparison with the purely conductive or purely magnetic anomalies. In the current paper, we develop a technique of interpreting the TDEM data over electrical inhomogeneous structures with potentially anomalous magnetic permeability.

Simultaneous inversion of EM data for magnetic permeability and conductivity has been investigated by only a few authors. Qian et al. (1996), and Beard and Nyquist (1996) calculated apparent resistivities and magnetic susceptibilities based on homogeneous half-space and two-layer models in the frequency

* Corresponding author. Fax: +1-801-581-7065.
*E-mail address:* mzhdanov@mines.utah.edu (M.S. Zhdanov).

0926-9851/01/$ - see front matter 
PII: S0926-9851(01)00041-6

domain. The method of simultaneous reconstruction of 1-D susceptibility and conductivity from frequency domain EM data for multi-layered models was developed recently by Zhang and Oldenburg (1999). Our approach is different from the cited papers, because, first, it is directed to interpretation of TDEM data, and, second, it is based on generalization of the *S*-inversion technique (Sidorov and Tikshaev, 1969; Tartaras and Zhdanov, 1996; Tartaras et al., 2000) for the models containing thin sheets with anomalous conductivity and anomalous magnetic permeability. We call this technique $S\mu$-inversion. It provides simultaneous inversion results for both conductivity and magnetic permeability distributions within geoelectrical cross-sections. The method can be used to detect magnetized geological structures, which can be of significant interest for exploration.

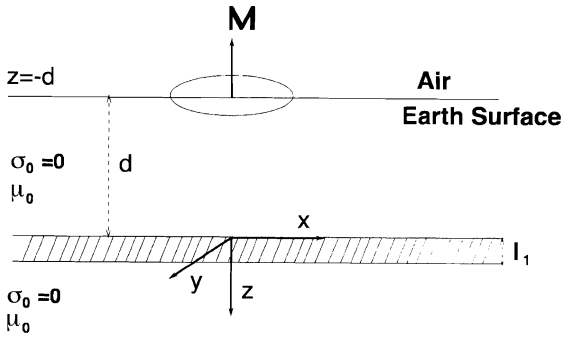


Fig. 1. Thin sheet model. Conductive thin sheet with a conductivity $\sigma_1$ and magnetic susceptibility $\chi = (\mu_1 - \mu_0)/\mu_0$ (where $\mu_0$ is a free space magnetic permeability, and $\mu_1$ is a magnetic permeability of the sheet) is located in nonconductive full space ($\sigma_0 = 0$). The time domain electromagnetic field in the model is excited by a vertical magnetic dipole, located on the earth's surface at the distance $d$ above the sheet. The origin of the Cartesian coordinate system is located on the top side of the sheet just beneath the magnetic dipole transmitter.

## 2. Electromagnetic field of a magnetic dipole above a thin conductive sheet with anomalous magnetic permeability

Let us examine the behavior of a step-induced transient magnetic field excited by a vertical magnetic dipole for a medium which consists of a single conducting thin sheet in an otherwise insulating full space (Fig. 1). We assume that an EM field is caused by current flowing in a loop of wire lying in the horizontal plane forming a vertical-axis magnetic dipole with a moment $M = M\mathbf{1}_Z$ ($\mathbf{1}_Z$ is a unit vector in the $Z$ direction) at a height, $d$, above a thin sheet with conductivity $\sigma_1$ and thickness $l_1$ (Fig. 1). The waveform of the current in the coil forming magnetic dipole moment $M$ is that of a Heaviside function (instantaneous change in level), $M = M_0 H(t)$. We wish to find the field from this source at the same height, $d$, above the sheet, this height being the surface of the earth where the source is situated and where the field is observed. We assume that the magnetic permeability of the medium is equal to free space permeability $\mu_0$, while the permeability of the sheet is $\mu_1$. We introduce also the magnetic susceptibility of the sheet, equal to

$$\chi = \mu_r - 1 = \frac{\mu_1}{\mu_0} - 1, \tag{1}$$

where $\mu_r = \mu_1/\mu_0$ is the relative permeability of the sheet.

We will use the technique of a spatial–time Fourier transform to solve the problem formulated above. The magnetic field at the surface of the earth ($z = -d$) caused by a source excited with a Heaviside (step on) wave form has the following Fourier representation (Zhdanov and Keller, 1994):

$$H_z(t)\big|_{z=-d} = \frac{1}{2\pi}\int_{-\infty}^{\infty}\frac{1}{4\pi^2}\int\int_{-\infty}^{\infty} h_z\big|_{z=-d} e^{-i(k_x x + k_y y)} dk_x dk_y \times \left\{\pi\delta(\omega) - \frac{1}{i\omega}\right\} e^{-i\omega t} d\omega, \tag{2}$$

where $h_z|_{z=-d}$ is a spatial spectrum of the vertical component of the magnetic field from the dipole source driven at a single harmonic frequency (the response for the actual Heaviside excitation is obtained by Fourier summation of frequencies). The expression for this spectrum is

$$h_z = -Mn_0^2 \frac{e^{-n_0 d} Z_\mu^*}{i\omega\mu_0 - n_0 Z_\mu^*}, \tag{3}$$

where $Z_\mu^*$ is the spectral impedance for the sequence lying beneath the plane $z = 0$ (Berdichevsky and

Zhdanov, 1984). For a single sheet shown in Fig. 1, the spectral impedance is equal to

$$Z_{\mu}^{*} = -\frac{i\omega\mu_1}{n_1}\coth\left[n_1 l_1 + \coth^{-1}\left(\frac{n_1\mu_0}{n_0\mu_1}\right)\right], \quad (4)$$

where $n_0 = (k_x^2 + k_y^2)^{1/2}$, $n_1 = (k_x^2 + k_y^2 - k_1^2)^{1/2}$, $k_1^2 = i\omega\mu_1\sigma_1$.

We assume now that we have an infinitesimal thin sheet with $l_1 \to 0$ and $\sigma_1 \to \infty$, $\chi \to \infty$, with the conductance $S$ and integrated susceptibility $X$ remaining constant:

$$\lim_{l_1 \to 0} \sigma_1 l_1 = S, \quad \text{and} \quad \lim_{l_1 \to 0} \chi l_1 = X. \quad (5)$$

In this particular problem, we will obtain a spectral impedance function by taking a limit for a two-layer sequence in which the conductivity of the sheet, $\sigma_1$, and magnetic susceptibility, $\chi = (\mu_1 - \mu_0)/(\mu_0)$, become large and at the same time its thickness, $l_1$, becomes vanishingly small.

Let us find the asymptotics of the spectral impedance $Z_{\mu}^{*}$ for infinitesimally thin sheet $l_1 \to 0$. Using the asymptotic condition that $lim_{x \to 0}\ x \coth x = 1$, we have

$$Z_{\mu}^{*} \approx -\frac{i\omega\mu_1}{n_1}\frac{1 + \dfrac{1}{n_1 l_1}\dfrac{n_1\mu_0}{n_0\mu_1}}{\dfrac{1}{n_1 l_1} + \dfrac{n_1\mu_0}{n_0\mu_1}}$$

$$= -i\omega\mu_0\frac{l_1(1+\chi)n_0 + 1}{n_0 - i\omega\mu_0\sigma_1 l_1}. \quad (6)$$

Substituting Eq. (6) into Eq. (3), we obtain

$$h_z\big|_{z=0} = Mn_0^2\frac{e^{-n_0 d}\left[l_1(1+\chi)n_0 + 1\right]}{\left[2n_0 + l_1(1+\chi)n_0^2 - i\omega\mu_0\sigma_1 l_1\right]}. \quad (7)$$

Thus, we find the spectrum of the total magnetic field on the surface of the conducting sheet. To find the spectrum of the internal part, we use the formula

$$h_z^{i}\big|_{z=0} = h_z\big|_{z=0} - h_z^{e}\big|_{z=0},$$

where $h_z^{e}$ is the spectrum of the vertical component of the external field in the absence of the conducting sheet, obtained from the Eq. (7) with $l_1 = 0$:

$$h_z^{e}\big|_{z=0} = \frac{1}{2}n_0 M e^{-n_0 d}. \quad (8)$$

Therefore, the spectrum of the internal field is

$$h_z^{i}\big|_{z=0} = \frac{1}{2}Mn_0 e^{-n_0 d}\frac{l_1(1+\chi)n_0^2 + i\omega\mu_0\sigma_1 l_1}{2n_0 + l_1(1+\chi)n_0^2 - i\omega\mu_0\sigma_1 l_1}.$$

Taking into account that we consider the asymptotics of the thin sheet model, $l_1 \to 0$, and using formula (5), we can further simplify the expression for the internal magnetic field:

$$h_z^{i}\big|_{z=0} \approx \frac{1}{2}Mn_0 e^{-n_0 d}\frac{Xn_0^2 + i\omega\mu_0 S}{2n_0 + Xn_0^2 - i\omega\mu_0 S}. \quad (9)$$

Using analytical continuation of the external and internal parts of the magnetic field upward, we obtain at the surface of the earth ($z = -d$)

$$h_z\big|_{z=-d} = h_z^{i}\big|_{z=0}e^{-n_0 d} + h_z^{e}\big|_{z=0}e^{+n_0 d}$$

$$= \frac{1}{2}Mn_0 e^{-2n_0 d}\frac{Xn_0^2 + i\omega\mu_0 S}{2n_0 + Xn_0^2 - i\omega\mu_0 S} + \frac{1}{2}n_0 M.$$

Applying an inverse Fourier transform, we find

$$H_z(t)\big|_{z=-d} = \frac{1}{2\pi}\int_{-\infty}^{\infty}\frac{1}{4\pi^2}\iint_{-\infty}^{\infty}h_z\big|_{z=-d}e^{[-i(k_x x + k_y y)]} \times dk_x dk_y\left\{\pi\delta(\omega) - \frac{1}{i\omega}\right\}e^{-i\omega t}d\omega$$

$$= \frac{I}{8\pi^2}\iint_{-\infty}^{\infty}n_0\left[A_1(t) + A_2(t) + A_3(t)\right] \times e^{[-i(k_x x + k_y y)]}dk_x dk_y, \quad (10)$$

where the integrals $A_1(t)$, $A_2(t)$, and $A_3(t)$ are introduced in Appendix A.

All of these integrals can be evaluated in a closed form. Lengthy but straightforward calculations, presented in Appendix A, lead to the following expression for the magnetic field, assuming $t > 0$:

$$H_z(t)\big|_{z=-d} = -\frac{M}{4\pi r^3} + \frac{M}{4\pi}\Big[\left(r^2+(2d+gt)^2\right)^{-5/2} \times\left(r^2-2(2d+gt)^2\right)\Big] - \frac{M}{4\pi}\frac{X}{2}\left(r^2+(2d+gt)^2\right)^{-7/2}(2d+gt) \times\left[-9r^2+6(2d+gt)^2\right], \quad (11)$$

where $g = 2/\mu_0 S$.

We can also write an expression for the time derivative of the magnetic field, because this physical quantity is usually measured by the induction loops

$$\frac{\partial H_z(t)}{\partial t}\bigg|_{z=-d} = \frac{M}{4\pi} g\left(r^2+(2d+gt)^2\right)^{-7/2}(2d+gt) \times\left[-9r^2+6(2d+gt)^2\right] - \frac{1}{8\pi}MXg\left(r^2+(2d+gt)^2\right)^{-9/2} \times\left[-9r^4+72r^2(2d+gt)^2-24(2d+gt)^4\right]. \quad (12)$$

Note in the conclusion that, in the case of the thin sheet with a magnetic permeability equal to free space permeability $\mu_1 = \mu_0$, we have $X = 0$, and formulae (11) and (12) reduce to the well-known expressions for the magnetic field response over a conductive thin sheet (Zhdanov and Keller, 1994) for $t > 0$:

$$H_z(t)\big|_{z=-d} = -\frac{M}{4\pi r^3} + \frac{M}{4\pi}\frac{r^2-8(d+t/\mu_0 S)^2}{\left[r^2+4(d+t/\mu_0 S)^2\right]^{5/2}}, \quad (13)$$

and

$$\frac{\partial H_z(t)}{\partial t}\bigg|_{z=-d} = \frac{M}{\pi\mu_0 S} \times\frac{(d+t/\mu_0 S)\left[-9r^2+24(d+t/\mu_0 S)^2\right]}{\left[r^2+4(d+t/\mu_0 S)^2\right]^{7/2}}. \quad (14)$$

Expressions (11)–(14) can be used for computing the TDEM response of the vertical magnetic dipole transmitter located over the thin sheet with the conductance $S$ and integrated susceptibility $X$.

## 3. Principles of $S\mu$-inversion

$S$-inversion is a fast-imaging technique for TDEM data interpretation based on the thin sheet model approach (Sidorov and Tikshaev, 1969; Tartaras and Zhdanov, 1996; Tartaras et al., 2000). We generalize this approach for simultaneous inversion for conductance $S$ and integrated susceptibility $X$.

The basic idea of the $S\mu$-inversion method is similar to $S$-inversion. The traditional approach to the interpretation of electrical sounding methods uses the concept of apparent resistivity. This concept is based on a simple model of a homogeneous half-space. We introduce the apparent resistivity $\rho_a$ as the

resistivity of the homogeneous half-space, which generates a theoretical EM response equal to the observed EM response for some frequency $\omega$ or for some time moment $t$ (for time domain electromagnetic field-TDEM). Thus, the apparent resistivity is a function of frequency $\rho_a(\omega)$ or time $\rho_a(t)$. In electromagnetic sounding theory, there are several well-known techniques, which transform the apparent resistivity curves into resistivity pseudosections. The idea is simple. We can introduce the effective depth of penetration $d$ of the EM field in the earth, which depends on frequency or time and is actually related to the skin-depth. After some algebraic transformation, one can derive the function of the apparent resistivity versus the effective depth $\rho_a(d)$. This curve describes a one-dimensional pseudosection beneath the sounding point.

In the case of $S\mu$-inversion, instead of considering equivalent homogeneous half-space, we introduce an equivalent conductive and at the same time magnetized thin sheet within the free space. We can determine the apparent conductance $S_a(t_1)$ and apparent integrated magnetic susceptibility $X_a(t_1)$ as the conductance and integrated susceptibility of the thin sheet located at the depth $d_1$ within the free space, which generates a theoretical EM response equal to the observed TDEM response for some time moment $t_1$. It is well known that the depth of TDEM field penetration is proportional to the square root of time $t$. Over time, the depth of penetration increases; therefore, the apparent total conductance $S_a(t_1)$ increases as well, because it is a monotonic function of the depth. Therefore, for the next time moment $t_2$ we will find another equivalent thin sheet with a greater conductance $S_a(t_2) > S_a(t_1)$ and a greater depth $d_2 > d_1$. Thus, the apparent conductance as well as the apparent integrated susceptibility are the functions of time, $S_a(t)$ and $X_a(t)$ The plots $S_a(t)$ and $X_a(t)$ are called apparent conductance and apparent integrated susceptibility curves. For every time moment, we find not only conductance and integrated susceptibility but also the depth $d$ of the equivalent thin sheet. Therefore, we can easily generate the functions of the apparent conductance and apparent integrated susceptibility versus the effective depth $S_a(d)$ and $X_a(d)$. Note that the conductance and integrated susceptibility of the geoelectrical cross-section are connected with the conductivity $\sigma(z)$ and magnetic susceptibility $\chi(z)$ distributions by simple formulae:

$$S(d) = \int_0^d \sigma(z)\,\mathrm{d}z,\ X(d) = \int_0^d \chi(z)\,\mathrm{d}z. \tag{15}$$

Therefore, by differentiating the conductance–depth and integrated susceptibility–depth curves, we can finally obtain the conductivity and susceptibility changes with the depth

$$\sigma(d) = \frac{\partial S(d)}{\partial d}, \tag{16}$$

$$\chi(d) = \frac{\partial X(d)}{\partial d}. \tag{17}$$

The relative magnetic permeability, $\mu_r$, of the medium is determined according to formula (1):

$$\mu_r(d) = 1 + \chi(d) = 1 + \frac{\partial X(d)}{\partial d}. \tag{18}$$

These curves describe the one-dimensional pseudosection beneath the sounding point. By combining these one-dimensional curves for different observation points, we obtain the conductivity cross-section $\sigma(x,d)$ and the relative permeability cross-section $\mu_r(x,d)$, where $x$ is the position of the observation point along the profile, and $d$ is the effective depth of the equivalent thin sheet, which varies from close to zero to some depth $D$, thus, outlining the geoelectrical cross-section. In this way, based on the observed time derivatives of the vertical component of the magnetic field, we can obtain the conductivity–depth and magnetic permeability–depth curves.

### 3.1. Regularized $S\mu$-inversion

Our approach to the solution of the inverse problem is based on full inversion with respect to the thin sheet parameters $S$, $X$, and $d$. We use an adaptive regularized conjugate-gradient inversion scheme to determine the thin sheet parameters.

Using Eq. (12) for the calculation of the field response, we fit the data measured at adjacent time channels in order to obtain the depth, conductance and integrated susceptibility of a thin sheet. Since we invert for three parameters, $S$, $X$, and $d$, we can use data from just three adjacent time channels for each

inversion. However, to make the solution more stable to noise, we select several adjacent time channels (usually 4–7) that form a sliding time window $(t - \Delta t/2,\ t + \Delta t/2)$, where $\Delta t$ is the width of the window (Fig. 2). Every fixed position of the sliding window center $t$ corresponds to the specific depth $z$ of the EM field penetration in the earth. We solve numerically the inverse problem and find the parameters of the thin sheet, $S$, $X$, and $d$. $d$ is equivalent to the thickness of the earth above some depth of penetration. When we move the sliding time window to later times, the new inverted parameters of the thin sheet correspond to the total thickness of the earth layers above the new depth of penetration. These values, $S(d)$, and $X(d)$, when plotted together, form the conductance–depth and integral magnetic permeability–depth curves.

We use the adaptive regularized conjugate-gradient method for the solution of the inverse problem (Zhdanov and Keller, 1994). It is based on minimization of the parametric functional

$$P^{\alpha}(m) = \phi(m) + \alpha s(m),$$

which is a linear combination of the misfit functional

$$\phi(m) = \| A(m) - D_{\text{obs}} \|^2,$$

and a stabilizing functional

$$s(m) = \| m - m_{\text{apr}} \|^2,$$

where $s(m)$ is used in order to ensure the stability of the inversion algorithm. In the above equations, $A(m)$ is the forward modeling operator, $D_{\text{obs}}$ is the observed TDEM data we are trying to fit, $m$ describes the parameters $S$, $X$, and $d$ of the thin sheet model, $m_{\text{apr}}$ is the a priori model, $\| \ldots \|$ denotes the least square norm, and $\alpha$ is the regularization parameter.

We use the conjugate gradient method to minimize the parametric functional. The iteration process

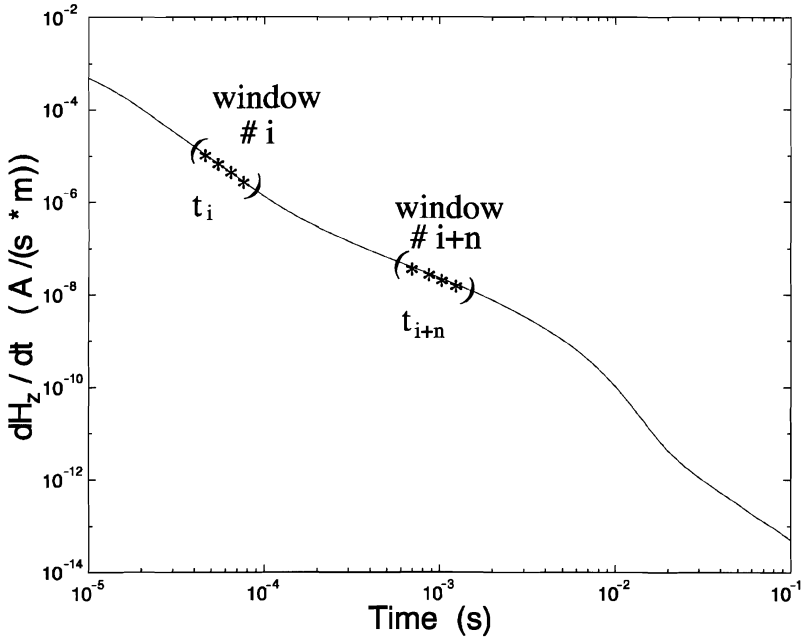


Fig. 2. Sliding time window in inversion scheme. The plot presents $(\partial H_z)/(\partial t)$ component behavior versus time of observation. We select several adjacent time channels (shown by stars) that form a sliding time window (shown by round brackets). Every fixed position of the sliding window center $t_i$ corresponds to the specific depth $z_i$ of the EM field penetration in the earth. We solve numerically the inverse problem for the observations $(\partial H_z)/(\partial t)$ within this window and find the parameters of the thin sheet, $S(z_i)$, $\mu(z_i)$, and $d(z_i)$, which is equivalent to the conducting thickness of the earth above the depth of penetration $z_i$. When we move the sliding time window to later times, $t_{i+n}$, the new inverted parameters of the thin sheet correspond to the total conductance and integrated susceptibility of the earth layer above the new depth of penetration $z_{i+n}$.

is automatically terminated when the normalized misfit reaches the desired value.

The Frechet derivative matrix, required for conjugate gradient algorithms, is composed of partial derivatives of data with respect to parameters. Thus, the Frechet matrix is an $N_d \times N_m$ matrix, where $N_d$ is the number of data points used and $N_m$ is the number of model parameters. Therefore, in our case the Frechet matrix is a $5 \times 3$ matrix, since we have three parameters (depth, $d$, integrated susceptibility, $X$, and conductance, $S$), and we usually use five-data points.

An important problem is the calculation of the appropriate value of the regularization parameter, $\alpha$. We use an adaptive regularization, which is based on the scaling down of the regularization parameter $\alpha$ after several subsequent iterations (Zhdanov, 1993). If the misfit value happens to increase, the value of $\alpha$ is decreased and the iteration step is repeated.

After we have determined the depth, conductance and integrated susceptibility values of the thin sheet for every time window, we differentiate the conductance and integrated susceptibility curves with respect to depth according to the formulae (16) and (17) to obtain the conductivity–depth and permeability–depth curves. The differentiating procedure is ill-posed and could produce instability in the solution. We apply spatial filtering to obtain stable results of differentiating.

Thus, as the result of $S\mu$-inversion, we generate conductivity–depth and magnetic permeability–depth profiles.

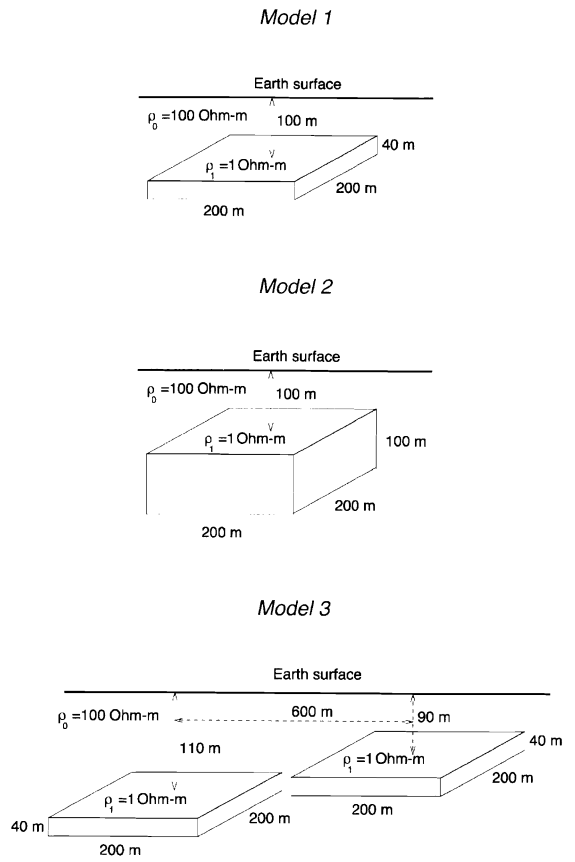


Fig. 3. 3-D geoelectrical models for testing $S\mu$-inversion: Model 1 with a thin conductive plate, Model 2 with a thick conductive plate, and Model 3 with two conductive plates at different depths. The background resistivity is of 100 Ω m, and the resistivity of the plates is of 1 Ω m. The plates have different relative magnetic permeability for different numerical tests. Both the transmitter and the receiver were vertical magnetic dipoles simulating horizontal induction loops located at the surface of the earth with 10-m separation. The Slingram mode was applied. Measurements were taken every 100 m along a profile passing above the center of the plate. The time interval of observations was between 1 μs and 1 s.

## 4. Application of $S\mu$-inversion to 3-D synthetic data interpretation

Three typical models are presented in Fig. 3. Model 1 (Fig. 3, top panel) consists of a horizontal rectangular plate with a horizontal size of $200 \times 200$ m$^2$ and a thickness of 40 m, located at a depth of 100 m within the homogeneous conductive half-space with a resistivity $\rho_1 = 100$ Ω m, and magnetic permeability of the free space $\mu_0$. Model 2 (Fig. 3, middle panel) consists of a thick rectangular plate with a horizontal size of $200 \times 200$ m$^2$ and a thickness of 100 m, located at a depth of 100 m within the homogeneous conductive half-space with the resistivity $\rho_1 = 100$ Ω m, and magnetic permeability of the free space $\mu_0$. Model 3 is presented in Fig. 3, bottom panel. It consists of two horizontal rectangular plates with a horizontal size of $200 \times 200$ m$^2$ and a thickness of 40 m, located at the different depths of 90 and 110 m within the homogeneous conductive half-space with the resistivity $\rho_1 = 100$ Ω m, and magnetic permeability of the free space $\mu_0$. We conducted a set of numerical experiments for these

models in which the relative permeability $\mu_r$ of the horizontal plates was equal subsequently to 1 and 5, and the plates were good conductors: $\rho_2 = 1\ \Omega$ m. The transient electromagnetic field in the model was generated by a step-wise pulse of electric current in a rectangular loop with a size of $50 \times 50$ m$^2$ located on the ground. Numerical modeling was conducted using the 3-D time domain finite-difference code developed by Wang and Hohmann (1993). The data used for $S\mu$-inversion was contaminated by 2% random noise.

First, we analyze Model 1. We studied the following two cases:

1. the horizontal plate is characterized by anomalous conductivity only (purely conductive anomaly); and
2. the horizontal plate has both anomalous magnetic permeability and anomalous conductivity (combined magnetic and conductive anomaly).

The numerical modeling code has been used to simulate a survey in Slingram mode with a central loop installation, where the transmitter and receiver were moving together along the profile and passing above the center of the 3-D structures. Measurements were taken every 25 m. It is assumed that the transmitter is excited by a step pulse and the receiver measures the time derivative of the magnetic field. The time interval of observations was between 10 μs and 10 ms.

Fig. 4, top panel, represents the conductivity cross-section obtained by the application of the $S\mu$-inversion at every receiver location for Model 1, shown in Fig. 3 (top panel), with a purely conductive anomaly. As we can see, the conductive body is satisfactorily imaged, although the retrieved conductivity is lower than the true one. Fig. 7, bottom panel, shows the relative magnetic permeability cross-section for the same model. As we could expect, this image shows practically no magnetic anomaly.

Fig. 5, top panel, presents the conductivity cross-section obtained by the application of the $S\mu$-inversion at every receiver location for Model 1, with a combined magnetic and conductive anomaly. Fig. 5, bottom panel, shows the relative magnetic permeability cross-section for the same model. One can see that the conductivity anomaly still corresponds well

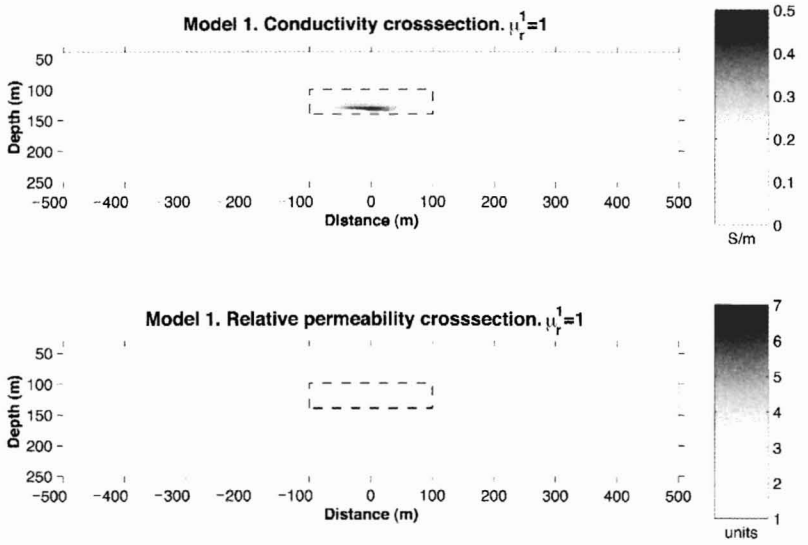


Fig. 4. Results of $S\mu$-inversion for Model 1 with the purely conductive plate (relative $\mu_r = 1$). The top panel represents a conductivity cross-section obtained by the application of the regularized $S\mu$-inversion at every receiver location along a profile passing above the center of the plate. The dashed line outlines the conductive plate. The bottom panel shows the relative magnetic permeability cross-section obtained by $S\mu$-inversion for the same model. As one should expect, this image shows practically no magnetic anomaly.

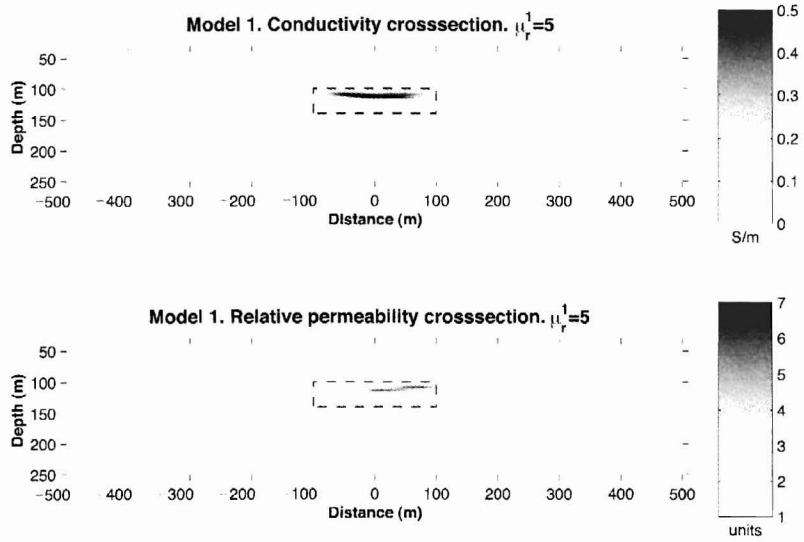


Fig. 5. Results of $S\mu$-inversion for Model 1 with a combined conductive and magnetic anomaly (relative $\mu_r = 5$). The top panel represents a conductivity cross-section obtained by the application of the regularized $S\mu$-inversion at every receiver location. The bottom panel shows the relative magnetic permeability cross-section obtained by $S\mu$-inversion for the same model. Both conductivity and magnetic permeability anomalies correspond well to the position of the plate shown by the dashed line.

to the position of the conductive body, while its magnitude practically does not change. At the same time, the image in Fig. 8, bottom panel, clearly demonstrates the presence of a magnetic anomaly, and the maximum of the retrieved relative magnetic permeability is close to the true one ( $\mu_r = 5$).

The second set of numerical experiments was applied to Model 2 (Fig. 3, middle panel). Fig. 6, top

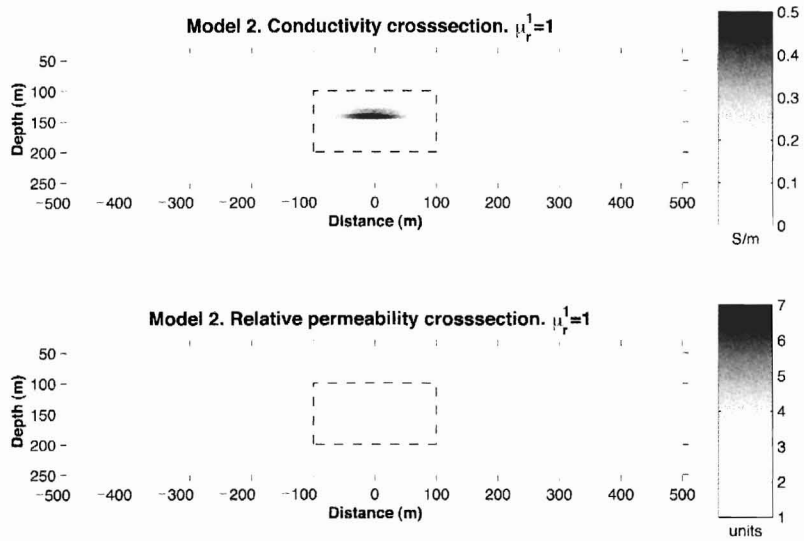


Fig. 6. Result of $S\mu$-inversion for Model 2 with the purely conductive plate (relative $\mu_r^1 = 1$). The top panel represents a conductivity cross-section obtained by the application of the regularized $S\mu$-inversion at every receiver location. The dashed line outlines the conductive plate. The bottom panel shows the relative magnetic permeability cross-section obtained by $S\mu$-inversion for the same model. As one should expect, this image shows practically no magnetic anomaly.

one equal to 1 S/m. The image in Fig. 6, bottom panel, shows practically no relative magnetic permeability anomaly, as one can expect for this model.

Fig. 7, top panel, presents the conductivity cross-section obtained by the application of the $S\mu$-inversion at every receiver location for the same model as above, but with a combined magnetic and conductive anomaly. Fig. 7, bottom panel, shows the relative magnetic permeability cross-section for the same model. One can see that the conductivity anomaly distribution outlines practically the entire anomalous body. The image in Fig. 7, bottom panel, clearly demonstrates the presence of a magnetic anomaly, and the retrieved relative magnetic permeability is close to the original $\mu_r = 5$.

The last set of numerical experiments was applied to Model 3 with two conductive plates (Fig. 3, bottom panel). Fig. 8, top panel, presents the conductivity cross-section obtained by the application of the $S\mu$-inversion at every receiver location for Model 3 with combined magnetic and conductive anomalies $\mu_r = 5$. Fig. 8, bottom panel, shows the relative magnetic permeability cross-section for the same model. One can see that the conductivity anomalies describe well the conductive plates, while the magnetic anomalies have values in the same range as the original $\mu_r = 5$.

In conclusion, based on the results of the above numerical modeling and inversion, we can say that $S\mu$-inversion seems to be a reliable and stable method for fast imaging of local conductive and magnetized targets and can separate the anomalous conductivity and magnetization effects in TDEM data.

## 5. Conclusions

We developed a new method of TDEM data interpretation, which allows simultaneous reconstruction of both electrical and magnetic properties of rocks. The method is based on generalization of the $S$-inversion technique (Tartaras and Zhdanov, 1996; Tartaras et al., 2000) for the models containing thin sheets with anomalous conductivity and anomalous magnetic permeability. We call this method $S\mu$-inversion. It provides simultaneous inversion results for both conductivity and magnetic permeability distributions within geoelectrical cross-sections.

Based on the results of 3-D modeling, we conclude that $S\mu$-inversion seems to be an efficient and stable method for fast imaging of anomalous conductive and magnetized geological structures using TDEM data. Furthermore, it is extremely fast because it does not require repetitive costly forward modeling.

The method of course has limitations. $S\mu$-inversion is an imaging technique, not a full conventional inversion. It usually underestimates the values of conductivity and magnetic permeability, so it works well in the case of strong anomalies.

Nevertheless, model study shows that $S\mu$-inversion can provide useful information about both subsurface conductivity and magnetic permeability distributions and can be treated as a new tool for imaging TDEM data in mineral exploration.

## Acknowledgements

The authors acknowledge the support of the University of Utah Consortium for Electromagnetic Modeling and Inversion (CEMI), which includes 3JTECH, Advanced Power Technologies, Agip, Baker Atlas Logging Services, BHP Minerals, EXXON Production Research, INCO Exploration, Japan National Oil Corporation, MINDECO, MOBIL Exploration and Production Technical Center, Naval Research Laboratory, Newmont Gold, Rio Tinto, Shell International Exploration and Production, Schlumberger-Doll Research, Unocal Geothermal, and Zonge Engineering.

The comments and suggestions of Drs. P. Weidelt and M. Asten are gratefully acknowledged.

## Appendix A. Derivation of the magnetic field of the magnetic dipole above a thin conductive sheet with anomalous magnetic permeability

We have demonstrated in Section 2 that the magnetic field of the magnetic dipole above a thin

conductive sheet with anomalous magnetic permeability can be expressed as an integral:

$$H_z(t)\big|_{z=-d_0} = \frac{1}{2\pi}\int_{-\infty}^{\infty}\frac{1}{4\pi^2}\int\int_{-\infty}^{\infty} h_z\big|_{z=-d_0} e^{[-i(k_x x+k_y y)]} \times dk_x dk_y \left\{\pi\delta(\omega)-\frac{1}{i\omega}\right\} e^{-i\omega t} d\omega = \frac{M}{8\pi^2}\int\int_{-\infty}^{\infty} n_0\left[A_1(t)+A_2(t)+A_3(t)\right] \times e^{[-i(k_x x+k_y y)]} dk_x dk_y, \quad (A.1)$$

where, assuming $t>0$, we have

$$A_1(t) = \frac{1}{2\pi}\int_{-\infty}^{\infty}\left\{\pi\delta(\omega)-\frac{1}{i\omega}\right\} e^{-i\omega t} d\omega = 1, \quad (A.2)$$

$$A_2(t) = -\mu_0 S e^{-2n_0 d}\frac{1}{2\pi}\int_{-\infty}^{\infty}\frac{e^{-i\omega t}}{2n_0+Xn_0^2-i\omega\mu_0 S} d\omega, \quad (A.3)$$

and

$$A_3(t) = Xn_0^2 e^{-2n_0 d}\frac{1}{2\pi}\int_{-\infty}^{\infty}\left\{\pi\delta(\omega)-\frac{1}{i\omega}\right\} \times \frac{e^{-i\omega t}}{2n_0+Xn_0^2-i\omega\mu_0 S} d\omega. \quad (A.4)$$

We can introduce an auxiliary integral

$$A_4(t) = Xn_0^2 e^{-2n_0 d}\frac{1}{2\pi}\int_{-\infty}^{\infty} \times \frac{e^{-i\omega t}}{2n_0+Xn_0^2-i\omega\mu_0 S} d\omega, \quad (A.5)$$

which satisfies the equation

$$\frac{\partial}{\partial t}A_3(t) = A_4(t). \quad (A.6)$$

The integral in Eqs. (A.3) and (A.5) can be evaluated using the tabulated form:

$$\frac{1}{2\pi}\int_{-\infty}^{\infty}\frac{p(\omega)}{f(\omega)} d\omega = -i\frac{p(\omega_0)}{\left.\frac{\partial f}{\partial\omega}\right|_{\omega_0}}, \quad (A.7)$$

where $p(\omega)=e^{-i\omega t}$, $f(\omega)=2n_0+Xn_0^2-i\omega\mu_0 S$, and $\omega_0$ is the kernel of the equation $f(\omega)=0$. It should be obvious that

$$\omega_0 = \left(2n_0+Xn_0^2\right)/i\mu_0 S. \quad (A.8)$$

Substituting Eq. (A.8) into Eq. (A.7), we find

$$\frac{1}{2\pi}\int_{-\infty}^{\infty}\frac{e^{-i\omega t}}{2n_0+Xn_0^2-i\omega\mu_0 S} d\omega = \frac{1}{2} g\exp\left(-\left(n_0+\frac{1}{2}Xn_0^2\right)gt\right),$$

where $g=(2)/(\mu_0 S)$.

Therefore,

$$A_2(t) = -\exp\left[-n_0\left(2d+\left(1+\frac{1}{2}Xn_0\right)gt\right)\right], \quad (A.9)$$

and

$$A_4(t) = \frac{1}{2} gXn_0^2\exp\left[-n_0\left(2d+\left(1+\frac{1}{2}Xn_0\right)gt\right)\right]. \quad (A.10)$$

According to Eq. (A.6),

$$A_3(t) = -\frac{1}{2}\frac{Xn_0}{\left(1+\frac{1}{2}Xn_0\right)} \times\exp\left[-n_0\left(2d+\left(1+\frac{1}{2}Xn_0\right)gt\right)\right]+C, \quad (A.11)$$

where $C$ is a constant.

As a result, we find

$$A_2(t)+A_3(t) = -\left[1+\frac{1}{2}\frac{Xn_0}{\left(1+\frac{1}{2}Xn_0\right)}\right] \times\exp\left[-n_0\left(2d+\left(1+\frac{1}{2}Xn_0\right)gt\right)\right]+C. \quad (A.12)$$

Considering Eqs. (A.4) and (A.12), we can write expression (A.1) for the magnetic field as

$$H_z(t)\big|_{z=-d_0} = \frac{M}{8\pi^2}\int\int_{-\infty}^{\infty} n_0\left[A_1(t)+A_2(t)+A_3(t)\right]e^{[-i(k_x x+k_y y)]}dk_x dk_y = \frac{M}{8\pi^2}B_1+\frac{M}{8\pi^2}CB_2-\frac{M}{8\pi^2}F(t). \quad (A.13)$$

In the last formula

$$B_1=-2\pi/r^3,$$

and

$$B_2=\int\int_{-\infty}^{\infty} n_0 e^{[-i(k_x x+k_y y)]}dk_x dk_y = \frac{1}{2\pi}\frac{\partial^2}{\partial z^2}\left(\frac{1}{R}\right)\Big|_{z=0} = -\frac{1}{2\pi r^3},$$

where $R=\sqrt{x^2+y^2+z^2}$, $r=\sqrt{x^2+y^2}$.

We have the following integral representation for expression $F(t)$:

$$F(t)=F_1(t)+F_2(t),$$

where functions $F_1(t)$ and $F_2(t)$ can be expressed by one integral $K(d,t)$:

$$F_1(t)=\frac{1}{4}\frac{\partial^2}{\partial d^2}K(d,t), \quad (A.14)$$

$$F_2(t)=-\frac{X}{8g}\frac{\partial}{\partial t}\frac{\partial^2}{\partial d^2}K(d,t), \quad (A.15)$$

and

$$K(d,t) = \int\int_{-\infty}^{\infty}\frac{1}{n_0}\exp\left[-n_0 a-n_0^2 b\right]\times e^{[-i(k_x x+k_y y)]}dk_x dk_y, \quad (A.16)$$

where $a=2d+gt$, $b=1/2\,Xgt$. Integral $K(d,t)$ can be evaluated using the Taylor's series:

$$K(d,t)=2\pi\int_0^{\infty}\frac{1}{n_0}\sum_{m=0}^{\infty}(-1)^m\frac{b^m n_0^{2m}}{m!}\times\exp[-n_0 a]e^{[-i(k_x x+k_y y)]}dk_x dk_y = 2\pi\sum_{m=0}^{\infty}(-1)^m\frac{b^m}{m!}\frac{d^{2m}}{da^{2m}}\left[\frac{1}{\sqrt{r^2+a^2}}\right].$$

Note that $a=2d+gt$ is big enough for the typical observation time, which usually exceeds 1 μs. Therefore, we can estimate the order of the derivatives in the last expression:

$$\frac{d^{2m}}{da^{2m}}\left[\frac{1}{\sqrt{r^2+a^2}}\right]\sim O\left(a^{-(2m+1)}\right)\sim O\left(gt^{-(2m+1)}\right).$$

Retaining the first term in the series, we obtain a simple formula

$$K(d,t)\approx\frac{2\pi}{\sqrt{r^2+(2d+gt)^2}}. \quad (A.17)$$

Substituting (Eqs. (A.14), (A.15) and (A.17) into Eq. (A.13), we find

$$H_z(t)\big|_{z=-d} = -\frac{M}{4\pi r^3}-\frac{M}{8\pi^2}\frac{1}{4}\frac{\partial^2}{\partial d^2}\left[\frac{2\pi}{\sqrt{r^2+(2d+gt)^2}}\right]+\frac{M}{8\pi^2}\frac{X}{8g}\frac{\partial}{\partial t}\frac{\partial^2}{\partial d^2}\left[\frac{2\pi}{\sqrt{r^2+(2d+gt)^2}}\right]. \quad (A.18)$$

Note that, for late time, $t\to\infty$, the magnetic field asymptotically tends to the static field, which satis-

fies the Biot–Savart law. Therefore, $C = 0$, and, after calculating the corresponding derivatives in formula (A.18), we finally obtain

$$H_z(t)\big|_{z=-d} = -\frac{M}{4\pi r^3} + \frac{M}{4\pi}\left[\left(r^2 + (2d+gt)^2\right)^{-5/2} \times \left(r^2 - 2(2d+gt)^2\right)\right] - \frac{M}{4\pi}\frac{X}{2}\left(r^2 + (2d+gt)^2\right)^{-7/2} \times (2d+gt)\left[-9r^2 + 6(2d+gt)^2\right]. \quad \text{(A.19)}$$

## References


Beard, L.P., Nyquist, J.E., 1996. Inversion of airborne electromagnetic data for magnetic permeability. 67th Annu. Int. Mtg., Soc. Expl. Geophys., Expanded Abstr., 940–943.

Berdichevsky, M.N., Zhdanov, M.S., 1984. Advanced Theory of Deep Geomagnetic Sounding. Elsevier, Amsterdam, Oxford, New York, Tokyo, 408 pp.

Pavlov, D.A., Zhdanov, M.S., 2001. Analysis and interpretation of anomalous conductivity and magnetic permeability effects in time domain electromagnetic data: Part I. Numerical modeling. J. Appl. Geophys. 46, 217–233.

Qian, W., Gamey, J., Lo, B., Holladay, J.S., 1996. AEM apparent resistivity and magnetic susceptibility calculation. 67th Annu. Int. Mtg., Soc. Expl. Geophys., Expanded Abstr., 1282–1285.

Sidorov, V.A., Tikshaev, V.V., 1969. Electrical Prospecting with Transient Field in Near zone. Saratov University, USSR.

Tartaras, E., Zhdanov, M.S., 1996. Fast S-inversion in the time domain: method of interpretation using the thin sheet approach. 66th Annu. Int. Mtg., Soc. Expl. Geophys., Expanded Abstr., 1306–1309.

Tartaras, E., Zhdanov, M.S., Wada, K., Saito, A., Hara, T., 2000. Fast imaging of TDEM data based on S-inversion. J. Appl. Geophys. 43, 15–32.

Wang, T., Hohmann, G.W., 1993. A finite-difference time domain solution for three-dimensional electromagnetic modeling. Geophysics 58, 797–809.

Zhang, Z., Oldenburg, D.W., 1999. Simultaneous reconstruction of 1-D susceptibility and conductivity from electromagnetic data. Geophysics 58, 33–47.

Zhdanov, M.S., 1993. Tutorial: Regularization in Inversion Theory. Colorado School of Mines, 47 pp.

Zhdanov, M.S., Keller, G.V., 1994. The Geo-electrical Methods in Geophysical Exploration. Elsevier, Amsterdam, Oxford, New York, Tokyo, 873 pp.